

Inversion of shape statistics for small solar system bodies

K. Muinonen^{1,2} and J.S.V. Lagerros¹

¹ Astronomical Observatory, Box 515, S-75120 Uppsala, Sweden (WWW: [Http://www.astro.uu.se/](http://www.astro.uu.se/))

² Observatory, P.O. Box 14, FIN-00014 University of Helsinki, Finland (WWW: <http://www.astro.helsinki.fi/>)

Received 10 December 1997 / Accepted 30 January 1998

Abstract. The irregular shapes of small solar system bodies are modelled by lognormal statistics, i.e., assuming that the shapes are realisations of the so-called Gaussian random sphere. The Gaussian sphere is fully described by the mean radius and the covariance function of the logarithmic radius. The stochastic shape is thus given by the covariance function, or the discrete spectrum of its Legendre coefficients. A maximum likelihood estimator is here provided for inverting the covariance function from three-dimensional sample shapes. The inverse method is applied to sophisticated shape data on altogether 14 small solar system bodies: the asteroids 4 Vesta, 243 Ida, 951 Gaspra, 1620 Geographos, 4179 Toutatis, and 4769 Castalia; the Martian satellites Phobos and Deimos; the Jovian satellite Amalthea; the Saturnian satellites Hyperion, Epimetheus, Janus, and Prometheus; and the Neptunian satellite Proteus. Inversion yields $\sigma = 0.245$ for the relative standard deviation of radius, shows that most of the spectral power lies in the second-degree spherical harmonics, and gives $\Gamma = 32.7^\circ$ for the correlation angle. Even though the first results are promising, caution is recommended because the number of sample shapes is still small. Omitting one sample shape at a time and repeating the inversion shows that the results are not too sensitive to any one sample shape.

As an example application, thermal light curves are simulated for 1 000 Gaussian sample spheres in order to study the uncertainties in diameters and masses derived for asteroids. As compared to the Standard Thermal Model that assumes spherical asteroids, the irregular shape is shown to cause a 5 % systematic effect with 10 % scatter in diameter estimation whereas, in mass estimation, the respective numbers are larger at 17 % and 33 %.

Key words: minor planets, asteroids – methods: analytical – methods: statistical

1. Introduction

We model the irregular shapes of small solar system bodies statistically as Gaussian spheres (e.g., Muinonen 1996, 1998; Lagerros 1997), and describe shapes of entire populations with a small number of parameters. Here we continue our earlier

introductory work and set out to derive statistical parameters from the three-dimensional shape models for small bodies. As to the shape models and their source, we refer the reader to Table 1.

Most comets and asteroids are small enough for their internal forces to withstand the deforming forces of gravity. As a result, some of them are highly irregularly shaped, as revealed by the images and radar maps available. The planetary sized satellites of the giant planets are essentially spherical, but the shapes become increasingly more irregular when moving to the smaller moons. The range of lightcurve amplitudes in the asteroid population (Lagerkvist et al. 1996) indicates a variety of shapes from almost spherical to highly elongated.

The shape is a historical record of impacts, catastrophic collisions, geological activity, cometary activity, or perhaps even the accretion of planetesimals in the early days of the solar system. The shape is also an important issue when comparing the distributions of mass, density, composition, and angular momentum between various populations of objects.

The shapes of minor bodies in the solar system are, however, difficult to investigate. There are space mission fly-by images of a few objects. Some near-Earth asteroids have been mapped by radar techniques. Most asteroid shapes, however, are currently only available as low order estimates from visual light curve investigations (Magnusson et al. 1989).

From another point of view, the shape is a complicating factor when determining other physical properties of asteroids and comets. Asteroids are usually modelled as spheres or ellipsoids. The impact of the irregular shapes on derived absolute magnitudes, albedos, diameters, lightcurve amplitudes, phase curves, etc. is poorly investigated. A large part of the problem is the difficulty to describe irregular shapes statistically.

The fundamental characteristics of lognormal distributions are given by Aitchison & Brown (1963). They provide a concise history for the distribution, and summarise the general properties of lognormal distributions, the most common one of them being the two-parameter distribution with the mean and standard deviation as parameters. What is relevant for the present study, they further describe the three-parameter distribution, where the third parameter, the threshold, defines a lower bound for the range of values of the lognormal random variable. Aitchison & Brown continue by describing the maximum likelihood

and other estimators for lognormal distributions, offer insight into hypothesis testing, and provide numerous applications of lognormal distributions, in particular, in economics. Aitchison & Brown show the multiplicative Central Limit Theorem for the lognormal distribution that supports the present, Gaussian shape hypothesis (Muinonen 1998).

The Gaussian random sphere has gradually matured during the past decade. Scattering of light by stochastically rough small particles was studied by Peltoniemi et al. (1989) in the ray optics approximation, that is, assuming that the particles were large compared to the wavelength of incident light. When continuing these scattering studies, Muinonen (1996) and Muinonen et al. (1996, 1997) devised a spherical harmonics representation for the stochastic shape, and introduced the term ‘Gaussian random sphere’ to pinpoint their specific class of stochastic shapes. The Gaussian random sphere has so far been applied, e.g., in the modelling of the shapes of asteroids (Lagerros 1997; Muinonen 1998) and the oscillations of raindrops (Nousiainen 1997; Nousiainen & Muinonen 1997), and as a model for the constituent grains in cosmic dust particles (Muinonen 1998).

The inverse problem of estimating the statistical parameters of the Gaussian random sphere from existing sample shapes has been addressed by Lamberg et al. (1997). They provide a maximum likelihood estimator for the Gaussian random sphere, a generalisation of that for the three-parameter lognormal distribution (Aitchison & Brown 1963). The key difficulty in the inverse problem concerns the geometric origins, with respect to which the sample shapes are given and assumed mathematically star-like. The origins are three-dimensional thresholds and required for individual shapes.

Lamberg et al. (1997) start from a set of two-dimensional sample intersections given with respect to certain origins, and iterate toward the maximum likelihood solution of the mean radius and the Fourier coefficients of the logradius covariance function and, simultaneously, the origins of the sample intersections. With the help of numerical simulations, they show that the method succeeds in solving the two-dimensional inverse problem. While formulating the maximum likelihood estimator for the three-dimensional inverse problem, Lamberg et al. (1997) do not provide practical, computational means for solving the inverse problem – such means are made available in the present paper.

Instead of self-similarity or fractal characteristics of shapes, we are primarily interested in shape irregularities in global and intermediate angular scales. It is evident that some of our model assumptions, e.g., that the shape can be given as a single-valued function with respect to a certain origin, break down at smaller angular scales. In terms of accuracy, the sample shapes form an inhomogeneous data set, and it is beyond the present study to account for these inhomogeneities. We do not account for craters in detail, but only note that separate crater modelling superimposed upon the overall shape would, in fact, result in increased freedom to model the shapes by the Gaussian random sphere.

In Sect. 2, we review the geometry and the maximum likelihood estimator of the Gaussian random sphere and, in

Sect. 3, describe some basic characteristics for individual three-dimensional shapes, distinguishing between translationally invariant and non-invariant properties. Sect. 4 contains the main results from the maximum likelihood estimation for the model statistical parameters. We analyse the sensitivity of the statistical parameters to the sample shapes, and provide an example application to asteroid diameter and mass estimation using thermal infrared lightcurves. Conclusions with suggestions for future work follow in Sect. 5.

2. Gaussian random sphere

The Gaussian random sphere and its maximum likelihood estimator are described in detail in Muinonen (1998) and Lamberg et al. (1997), respectively. The size and shape of the Gaussian sphere are described by the mean radius and the covariance function of the logarithmic radius. The covariance function is given as series of Legendre polynomials with non-negative coefficients. For each degree, these coefficients provide the spectral weights of the corresponding spherical harmonics components in the Gaussian sphere. Weighting the spectrum toward higher-degree harmonics will result in Gaussian sample spheres with larger numbers of hills and valleys as per solid angle. Increasing the variance of the logarithmic radius will enhance the hills and valleys radially. In what follows, brief summaries are given on the most essential aspects of the Gaussian sphere and its maximum likelihood estimator.

2.1. Statistical model

The three-dimensional Gaussian random sphere $r = r(\vartheta, \varphi)$ is described by the spherical harmonics (Laplace) series for the so-called logradius $s = s(\vartheta, \varphi)$ (Muinonen 1996),

$$\begin{aligned} r(\vartheta, \varphi) &= a \exp \left[s(\vartheta, \varphi) - \frac{1}{2} \beta^2 \right], \\ s(\vartheta, \varphi) &= \sum_{l=0}^{\infty} \sum_{m=-l}^l s_{lm} Y_{lm}(\vartheta, \varphi), \end{aligned} \quad (1)$$

where a and β are the mean radius and the standard deviation of the logradius, and Y_{lm} 's are the orthonormal spherical harmonics with Condon-Shortley phase (Arfken 1970). The relative standard deviation of radius is $\sigma = \sqrt{\exp(\beta^2) - 1}$, and depends solely on β . The logradius is real-valued so that

$$\begin{aligned} s_{l,-m} &= (-1)^m s_{lm}^*, \\ l &= 0, 1, \dots, \infty, \quad m = -l, \dots, -1, 0, 1, \dots, l, \end{aligned} \quad (2)$$

implying $\text{Im}(s_{l0}) \equiv 0$.

The real and imaginary parts of the spherical harmonics coefficients s_{lm} , $m \geq 0$, are independent Gaussian random variables with zero means and variances

$$\begin{aligned} \text{Var}(\text{Re}(s_{lm})) &= (1 + \delta_{m0}) \frac{2\pi}{2l+1} C_l, \\ \text{Var}(\text{Im}(s_{lm})) &= (1 - \delta_{m0}) \frac{2\pi}{2l+1} C_l, \\ l &= 0, 1, \dots, \infty, \quad m = 0, 1, \dots, l. \end{aligned} \quad (3)$$

The coefficients $C_l \geq 0$ ($l = 0, \dots, \infty$) are the Legendre coefficients of the logradius covariance function Σ_s ,

$$\Sigma_s(\gamma) = \beta^2 C_s(\gamma) = \sum_{l=0}^{\infty} C_l P_l(\cos \gamma),$$

$$\sum_{l=0}^{\infty} C_l = \beta^2, \quad (4)$$

where C_s is the logradius correlation function,

$$C_s(\gamma) = \sum_{l=0}^{\infty} c_l P_l(\cos \gamma),$$

$$\sum_{l=0}^{\infty} c_l = 1. \quad (5)$$

In practice, the series representations in Eqs. (1), (4), and (5) need to be truncated at a certain degree L sufficiently high to maintain good precision in the generation of sample spheres.

The two perpendicular slopes

$$s_\vartheta = \frac{r_\vartheta}{r}, \quad \frac{1}{\sin \vartheta} s_\varphi = \frac{r_\varphi}{r \sin \vartheta}, \quad (6)$$

are independent Gaussian random variables with zero means and standard deviations

$$\rho = \sqrt{-\Sigma_s^{(2)}(0)}, \quad (7)$$

where $\Sigma_s^{(2)}$ is the second derivative of the covariance function with respect to γ . The correlation length ℓ and correlation angle Γ are defined by

$$\ell = \frac{1}{\sqrt{-C_s^{(2)}(0)}},$$

$$\Gamma = 2 \arcsin\left(\frac{1}{2}\ell\right). \quad (8)$$

2.2. Maximum likelihood estimator

According to Lamberg et al. (1997) but omitting the mean radius estimation, the probability density (or likelihood) function for the $L + 1$ Legendre coefficients $\{C_l\}$ and the origins $\{\mathbf{r}_n\}$ of the N sample shapes can be written as

$$p(\{C_l\}, \{\mathbf{r}_n\}) \propto \prod_{n=1}^N \exp\left[-\frac{1}{2} \sum_{l=0}^L (2l+1) \left(\frac{\tilde{C}_{ln}(\mathbf{r}_n)}{C_l} + \log_e C_l\right)\right], \quad (9)$$

where the Legendre coefficients $\tilde{C}_{ln}(\mathbf{r}_n)$ pertain to individual sample shapes,

$$\tilde{C}_{ln}(\mathbf{r}_n) = \frac{2l+1}{4\pi} \frac{1}{l+1} \sum_{m=0}^l |s_{lm}(\mathbf{r}_n)|^2. \quad (10)$$

A constraint on the location of the origin is the requirement that the shape be mathematically star-like with respect to the origin.

The inverse problem of estimating the model parameters consists of finding those $\{C_l\}$ and $\{\mathbf{r}_n\}$ that maximise the likelihood function in Eq. (9). The total number of parameters thus amounts to $L + 1 + 3N$. For given origins $\{\mathbf{r}_n\}$, it is straightforward to show that the Legendre coefficients maximising the likelihood function coincide with the means of the coefficients for the individual sample shapes,

$$C_l = \frac{1}{N} \sum_{n=1}^N \tilde{C}_{ln}(\mathbf{r}_n). \quad (11)$$

In practice, the final maximum likelihood solution for the parameters can be obtained gradually by, first, computing estimates for the Legendre coefficients from Eq. (11) and, second, improving the origins by using the new Legendre coefficients in Eq. (9), and repeating the procedure until changes in the origins and the Legendre coefficients become negligible. Whenever the origin of a sample shape changes, new spherical harmonics coefficients are needed for the computation of the Legendre coefficients in Eq. (11), which constitutes a considerable computational challenge in the application of the maximum likelihood estimator.

3. Individual shape characteristics

3.1. Translational invariants

The volume V , surface area A , and total surface curvature K are useful translationally invariant quantities for an individual sample shape. The overall dimensions of the shape can be described by the invariant equal-volume-sphere and equal-area-sphere radii

$$a_V = \sqrt[3]{\frac{3V}{4\pi}},$$

$$a_A = \sqrt{\frac{A}{4\pi}}. \quad (12)$$

With the help of the total curvature, the total solid angle swept by the surface normal can be computed as

$$\Omega = \oint_S dS |K|. \quad (13)$$

For convex bodies, the solid angle $\Omega = 4\pi$ whereas, for concave bodies, it always holds that $\Omega > 4\pi$. The translational invariants a_V , a_A , and Ω can be used in the maximum likelihood estimation to monitor whether the sample shapes remain star-like for changing origins.

We make use of three invariant origins that are associated with the volume, area, and curvature,

$$\mathbf{r}_V = \frac{1}{V} \int_V dV \mathbf{r},$$

$$\mathbf{r}_A = \frac{1}{A} \oint_S dS \mathbf{r}, \quad (14)$$

$$\mathbf{r}_\Omega = \frac{1}{\Omega} \oint_S dS |K| \mathbf{r}.$$

The first origin coincides with the centre of mass for a body with constant density, while the second is the centre of mass for a hollow body with constant surface density. The third origin can be termed the angular origin (Eq. 13). The origins in Eq. (14) can be used to initialise the maximum likelihood estimator for the Gaussian random sphere. However, the shapes are not necessarily star-like with respect to these origins, a possibility that needs to be checked before starting the maximum likelihood estimation.

3.2. Intrinsic statistics

It is useful to define statistical parameters that are intrinsic properties of individual shapes $r = r(\vartheta, \varphi)$ described by the radius vector

$$\mathbf{r}(\vartheta, \varphi) = r(\vartheta, \varphi)(\sin \vartheta \cos \varphi, \sin \vartheta \sin \varphi, \cos \vartheta)^T \quad (15)$$

with respect to a given origin. In order to distinguish between individual and ensemble statistical parameters, we make use of ‘tilde’ in connection to the parameters for individual shapes. Note that, in Eq. (9–11), such a convention was already followed for the Legendre coefficients of the individual covariance functions.

Most of the key statistical parameters for an individual sample shape depend on the coordinate system. Let us start by defining the intrinsic expectation – if $f = f(\vartheta, \varphi)$ is given relative to some origin, the expectation of f is

$$E(f) = \frac{1}{4\pi} \int_0^\pi \int_0^{2\pi} d\vartheta d\varphi \sin \vartheta f(\vartheta, \varphi). \quad (16)$$

The mean radius $\tilde{\alpha}$, the relative standard deviation of radius $\tilde{\sigma}$, the standard deviation of the logarithmic radius $\tilde{\beta}$, and the standard deviation of slopes $\tilde{\rho}$ for an individual shape are

$$\begin{aligned} \tilde{\alpha} &= E(r), \\ \tilde{\sigma}^2 &= \frac{1}{\tilde{\alpha}^2} [E(r^2) - E(r)^2], \\ \tilde{\beta}^2 &= E[(\log_e r)^2] - [E(\log_e r)]^2 \\ \tilde{\rho}^2 &= \frac{1}{2} E \left(\frac{r_\vartheta^2}{r^2} + \frac{r_\varphi^2}{r^2 \sin^2 \vartheta} \right). \end{aligned} \quad (17)$$

Furthermore, the standard deviations of radius and slope can be related to a correlation angle $\tilde{\Gamma}$ that partly characterises the correlation function for an individual shape. We define $\tilde{\Gamma}$ as

$$\tilde{\Gamma} = 2 \arcsin \frac{\sqrt{\log_e(1 + \tilde{\sigma}^2)}}{2\tilde{\rho}} \quad (18)$$

For small $\tilde{\sigma}$, the approximation $\tilde{\Gamma} \approx \tilde{\sigma}/\tilde{\rho}$ is useful.

4. Results and discussion

4.1. Irregular shapes of the solar system

The irregular shapes of the moons and minor bodies used here were collected from a number of sources as indicated in Table 1. There are maps and low order shape estimates of many

more irregular objects, but here the goal is to characterise the detailed 3-dimensional shapes of irregular solar system bodies. The available sample is therefore small and inhomogeneous. Both the type of objects and quality of the data varies significantly within the dataset.

This dataset is fascinating since it is based on a large variety of techniques. It is clearly beyond the scope of this paper to discuss all these methods in full detail and the possible implications on the quality of the dataset. The shapes are taken as they are given by the authors, with the following considerations in mind:

Direct imaging: mid- to high resolution images have been provided by the Viking orbiter, Voyager 1 & 2, Galileo and the Hubble Space Telescope. The shape models are based on fitting limb profiles and using various surface features as geometric control points. The resolution varies substantially and the coverage is sometimes incomplete for some of the objects.

Radar mapping: the delay of the reflected signal from some part of the surface gives the range to the Earth, while the Doppler shift measures the position relative to the projected spin vector. In order to derive a 3-D shape model, somewhat elaborate modelling is required.

The geometric centre (Eq. 14, centre of mass assuming constant density) was calculated for each shape. It did not always agree with the origin of the provided coordinate systems. To make the data set as consistent as possible, all shapes were re-centred to the geometric centre.

In Table 2, the statistical parameters of Sect. 3.2 are given for the 14 shapes, using the three different origins. The shapes were carefully verified to be star-like with respect to all three origins. Note how the mean radius systematically decreases from left to right in the table, while the other parameters increase.

As seen from Fig. 1, the shapes seem to follow the same simple $\tilde{\sigma}$ - $\tilde{\rho}$ relation. Part of it is no surprise since a large $\tilde{\sigma}$ implies a large $\tilde{\rho}$, and vice versa, but *a priori* there is no apparent reason to expect essentially the same $\tilde{\sigma}/\tilde{\rho}$ ratio over almost three orders of magnitude in size. If the outlier Proteus is removed, the mean correlation angle is $28^\circ \pm 3^\circ$. (Note that this mean angle is not to be confused with the ensemble correlation angle.)

The standard deviation $\tilde{\sigma}$ correlates with the size of the object, as seen in Fig. 2. For the two populations of small and large objects (excluding 243 Ida), it is possible to fit

$$\tilde{\sigma}_{\text{small}} = 0.32 - 0.15 \lg(\tilde{\alpha}/1 \text{ km})$$

$$\tilde{\sigma}_{\text{large}} = 0.49 - 0.18 \lg(\tilde{\alpha}/1 \text{ km})$$

As expected, the shapes become more spherical with increasing size. Although there is a difference between the two populations, the fitted values of $d\tilde{\sigma}/d(\lg \tilde{\alpha})$ are quite similar over a large range of sizes.

In Fig. 3, we show the logradius covariance functions $\tilde{\Sigma}_s$ for individual sample shapes computed with respect to the angular origins (Eq. 14). It is 243 Ida that exhibits the largest surface

Table 1. Sample shapes with references and translationally invariant properties (Sect. 3.1). We give the radii for equal-volume (a_V) and equal-area spheres (a_A), and the solid angles ($\Omega \geq 4\pi$) swept by the surface normals.

Object	Reference	a_V (km)	a_A (km)	a_A/a_V	$\Omega/4\pi$
4769 Castalia	Hudson & Ostro (1994)	0.55	0.59	1.083	2.263
4179 Toutatis	Hudson & Ostro (1995)	1.19	1.30	1.087	2.278
1620 Geographos	Stooke (1997)	1.20	1.31	1.099	1.585
951 Gaspra	Thomas et al. (1994)	6.10	6.44	1.055	1.711
Deimos	Thomas (1989)	6.24	6.42	1.029	1.224
Phobos	Thomas (1989)	11.11	11.32	1.019	1.252
243 Ida	Thomas et al. (1996)	15.66	17.48	1.116	2.559
Prometheus	Stooke (1993a)	45.27	48.32	1.067	1.655
Epimetheus	Stooke (1993b)	57.47	59.16	1.029	1.629
Amalthea	Stooke (1992)	81.83	86.08	1.052	1.641
Janus	Stooke & Lumsdon (1993)	89.08	90.35	1.014	1.137
Hyperion	Thomas et al. (1995)	131.60	134.65	1.023	1.193
Proteus	Stooke (1994)	201.22	203.97	1.014	1.323
4 Vesta	Thomas et al. (1997), Stooke (1997)	254.65	256.46	1.007	1.034

Table 2. Statistical properties of the sample shapes with respect to three different origins (Sect. 3.2).

Object	Volume origin \tilde{r}_V				Areal origin \tilde{r}_A				Angular origin \tilde{r}_Ω			
	\tilde{a} (km)	$\tilde{\sigma}$	$\tilde{\rho}$	$\tilde{\Gamma}$ ($^\circ$)	\tilde{a} (km)	$\tilde{\sigma}$	$\tilde{\rho}$	$\tilde{\Gamma}$ ($^\circ$)	\tilde{a} (km)	$\tilde{\sigma}$	$\tilde{\rho}$	$\tilde{\Gamma}$ ($^\circ$)
4769 Castalia	0.50	0.293	0.581	28.6	0.50	0.296	0.585	28.7	0.50	0.304	0.593	29.0
4179 Toutatis	1.10	0.280	0.533	29.9	1.09	0.298	0.551	30.7	1.06	0.351	0.597	33.2
1620 Geographos	1.08	0.319	0.546	33.1	1.08	0.321	0.549	33.1	1.06	0.353	0.587	33.9
951 Gaspra	5.84	0.210	0.408	29.5	5.83	0.217	0.415	29.9	5.77	0.240	0.434	31.6
Deimos	6.13	0.135	0.304	25.5	6.12	0.138	0.310	25.6	6.04	0.190	0.374	29.2
Phobos	11.00	0.102	0.229	25.8	11.00	0.103	0.230	25.9	10.96	0.121	0.244	28.7
243 Ida	13.64	0.398	0.861	25.7	13.54	0.414	0.898	25.6	13.41	0.431	0.933	25.6
Prometheus	43.03	0.226	0.441	29.3	43.03	0.226	0.441	29.3	42.82	0.238	0.450	30.2
Epimetheus	56.63	0.121	0.281	24.9	56.63	0.122	0.281	24.9	56.60	0.124	0.283	25.2
Amalthea	78.97	0.187	0.384	28.0	78.92	0.189	0.386	28.1	78.41	0.207	0.404	29.4
Janus	88.40	0.088	0.196	26.0	88.40	0.089	0.196	26.0	88.34	0.092	0.199	26.8
Hyperion	129.22	0.136	0.263	29.8	129.20	0.136	0.264	29.8	128.91	0.145	0.273	30.7
Proteus	200.69	0.051	0.181	16.3	200.68	0.052	0.181	16.4	200.35	0.066	0.189	20.2
4 Vesta	253.39	0.071	0.145	28.5	253.39	0.071	0.145	28.5	253.36	0.072	0.145	28.7

variations among the 14 bodies. Fig. 4 shows the individual correlation functions. Note the similarity of the correlation functions, underscoring and extending the similarity in Fig. 1.

4.2. Maximum likelihood estimates

The maximum likelihood estimator was carefully verified for simulated Gaussian sample spheres: the inversion method worked in a satisfactory way even for small numbers of sample shapes comparable to the number of small bodies' shapes currently included in the data set.

First estimates for the Legendre coefficients of the log-radius covariance function were obtained from the spherical harmonics coefficients computed with respect to the angular origin (Sect. 3). By varying the origins of the sample shapes and monitoring the translational invariants (Sect. 3.1), all the shapes were

concluded to be star-like with respect to their angular origins. It is important to note that the sample shapes were first expressed as pure exponentials of spherical harmonics series, whereafter their spherical harmonics coefficients s_{00} , including the size of the bodies, were set to zero. Such preconditioning resulted in a size-wise homogeneous data set.

The first estimates computed with respect to the volume or areal origins deviated considerably from the final maximum likelihood estimates, whereas the first estimate computed with respect to the angular origins was rather close to the final maximum likelihood estimate. Thus, in order to obtain reasonable first estimates for the Legendre coefficients, the angular origins are recommended though their computation is somewhat more demanding.

The maximum degree used throughout the study was $L = 10$. The two-dimensional numerical integrations for the spher-

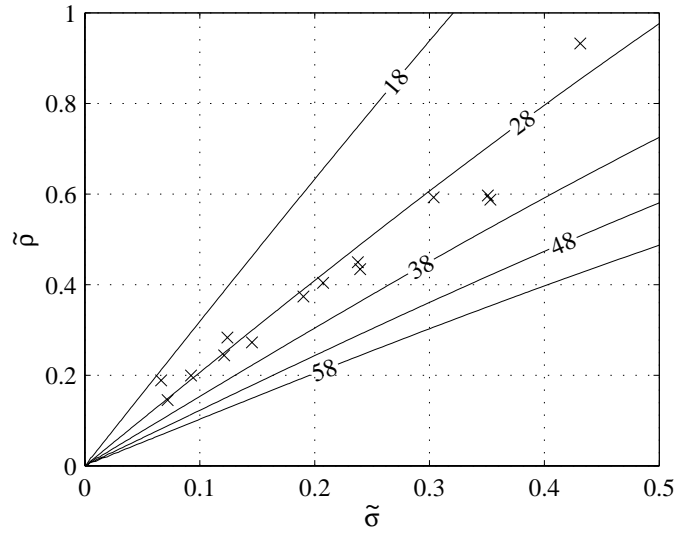


Fig. 1. The standard deviation of slope $\tilde{\rho}$ against the relative standard deviation of the radius $\tilde{\sigma}$ for the 14 individual shapes in Table 2 using the angular origins r_Ω . Lines are drawn for $\Gamma = 18^\circ, 28^\circ, 38^\circ, 48^\circ$, and 58° , using Eq. (18).

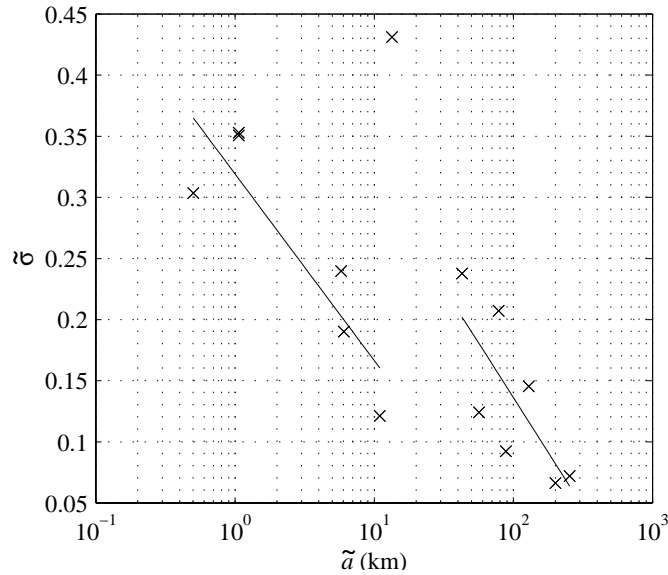


Fig. 2. The relative standard deviation $\tilde{\sigma}$ versus the mean radius \tilde{a} using the angular origins r_Ω . Lines are fitted to the two populations (243 Ida excluded).

ical harmonics coefficients were carried out by using Gauss-Legendre abscissae and weights for the cosine of the polar angle, and uniform abscissae and weights for the azimuthal angle. Final refinement of the statistical parameters was carried out by using 120 integration points for the cosine of the polar angle, and 360 integration points for the azimuthal angle. The present numerical computations took several weeks of computing time on a modern workstation.

The search for maximum likelihood estimates of the ensemble statistical parameters and the individual origins was carried out gradually. For a certain set of Legendre coefficients of the lo-

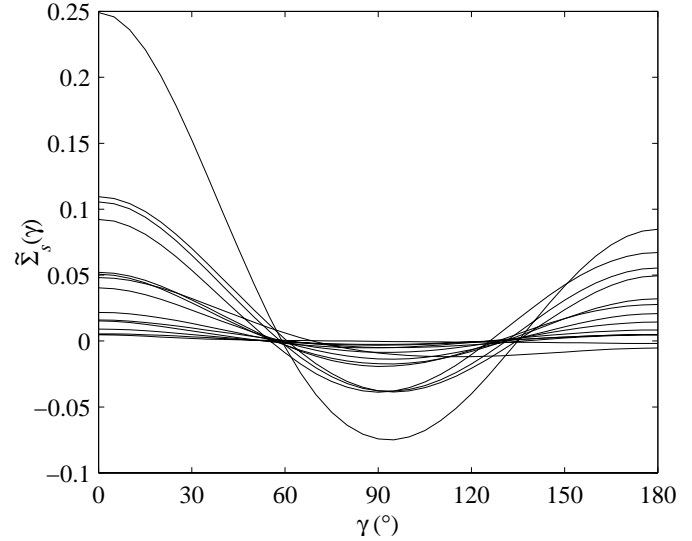


Fig. 3. The individual logradius covariance functions $\tilde{\Sigma}_s(\gamma)$ for the 14 sample shapes. Computed with respect to the r_Ω -origin.

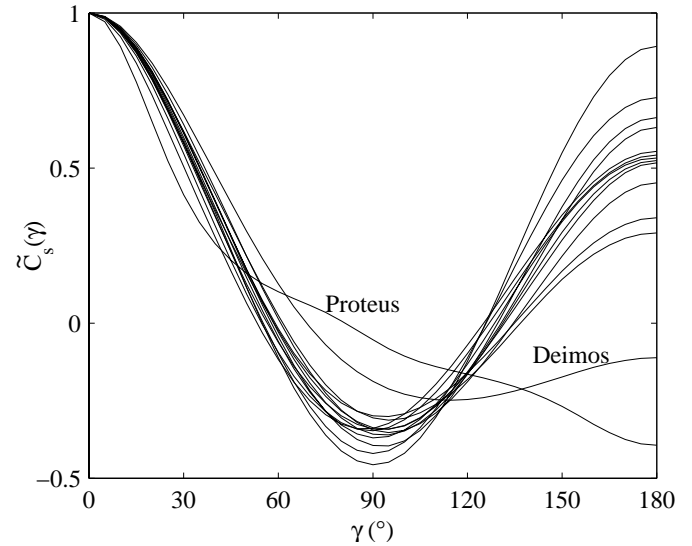


Fig. 4. The individual logradius correlation functions $\tilde{C}_s(\gamma)$ for the 14 sample shapes. Computed with respect to the r_Ω -origin.

gradius correlation function, a new set of origins were computed for the sample shapes by using downhill simplex minimisation. The convergence criterion for the origins was set at 10^{-3} (maximum size of the simplex in units of length for preconditioned shapes, see above) and, for the overall convergence of the exponential argument in Eq. (9), the tolerance was fixed at 10^{-6} .

No significant problems were encountered in the application of the maximum likelihood estimator to the sample shapes. The translationally invariant quantities in Table 1 were used in order to check that the shapes were star-like with respect to the final origins. That was noted to be the case for all others but 4179 Toutatis and 243 Ida, for which the final equal-volume-sphere and equal-area-sphere radii a_V and a_A were in close agreement with the original values, whereas the angular metrics Ω deviated markedly from the original values. Some high-

Table 3. The standard deviations of radius (relative), logradius, and slope σ , β , and ρ , respectively, and the correlation angle Γ . Inverted using all 14 shapes, and the groups of 7 largest and 7 smallest bodies.

	All	Large	Small
σ	0.245	0.241	0.274
β	0.241	0.238	0.269
ρ	0.428	0.345	0.505
Γ	32.7°	40.4°	30.9°

degree features on the surfaces of these two bodies could not be expressed with respect to the final origins. However, recalling the inhomogeneous accuracy of the data set and the mild violation of star-likeness, no measures were taken to enforce the origins inside the star-likeness regimes. Furthermore, the omission of either one of these shapes from the data set did not affect the final maximum likelihood estimates significantly.

In what follows, we present results for inversion with all 14 observed shapes, and with the 7 smallest and the 7 largest shapes (Tables 3-5). The sensitivity of the 14-shape maximum likelihood estimates was studied with the help of the Quenouille-Tukey jackknife method (Babu & Feigelson 1996) by omitting one sample shape at a time, and repeating the maximum likelihood estimation for the remaining 13 shapes. The resulting covariance and correlation functions are shown in Figs. 5 and 6 with error envelopes determined by the maximum deviations resulting from the omission procedure above. In Figs. 5 and 6, we also give the covariance and correlation functions from direct computation with respect to the angular origins, that is, the initial functions before improvement via iteration.

Fig. 7 shows sample shapes simulated using the Legendre coefficients from the inversion procedure for the 14 sample shapes. The shapes are reasonable, although the real shapes appear to be more edge-shaped than the smoother Gaussian counterparts. The inversion for the 7 smallest and the 7 largest bodies results in differing covariance functions, although the variances were quite similar. When comparing the estimates for the 14 shapes and the 7 largest shapes, it is interesting to note the similarity of the logradius standard deviations, and the rough exchange of the roles of the C_1 and C_2 Legendre coefficients. The C_2 -contribution predominates for the case of 14 shapes, and it increases for decreasing size of the bodies.

4.3. Example application

The shape of most asteroids is difficult and tedious to obtain by today's techniques. With the shape model proposed here it is on the other hand possible to statistically investigate shape effects. For example, the Standard Thermal Model (STM) (Lebofsky & Spencer 1989, and references therein) is a popular model for determining the diameters of asteroids. In STM, the asteroids are approximated by spheres, and the question is if this highly approximate assumption is causing any systematic errors when estimating for example diameters.

Table 4. The Legendre coefficients C_l of the logradius covariance function $\Sigma_s(\gamma)$. Classes as in Table 3.

l	All	Large	Small
0	$1.0868 \cdot 10^{-3}$	$4.2531 \cdot 10^{-3}$	$6.9066 \cdot 10^{-4}$
1	$1.9781 \cdot 10^{-2}$	$3.4049 \cdot 10^{-2}$	$1.5902 \cdot 10^{-2}$
2	$3.0082 \cdot 10^{-2}$	$1.4763 \cdot 10^{-2}$	$4.5353 \cdot 10^{-2}$
3	$3.8134 \cdot 10^{-3}$	$1.3026 \cdot 10^{-3}$	$6.0555 \cdot 10^{-3}$
4	$1.8170 \cdot 10^{-3}$	$1.2252 \cdot 10^{-3}$	$2.2904 \cdot 10^{-3}$
5	$7.4273 \cdot 10^{-4}$	$3.2945 \cdot 10^{-4}$	$1.1226 \cdot 10^{-3}$
6	$4.1604 \cdot 10^{-4}$	$4.1814 \cdot 10^{-4}$	$4.8764 \cdot 10^{-4}$
7	$1.3700 \cdot 10^{-4}$	$5.5142 \cdot 10^{-5}$	$1.9496 \cdot 10^{-4}$
8	$1.4028 \cdot 10^{-4}$	$6.4142 \cdot 10^{-5}$	$2.0762 \cdot 10^{-4}$
9	$4.0766 \cdot 10^{-5}$	$3.9760 \cdot 10^{-5}$	$4.1202 \cdot 10^{-5}$
10	$1.9810 \cdot 10^{-5}$	$1.7243 \cdot 10^{-5}$	$2.8242 \cdot 10^{-5}$

Table 5. The Legendre coefficients c_l of the logradius correlation function $C_s(\gamma)$. Classes as in Table 3.

l	All	Large	Small
0	$1.8714 \cdot 10^{-2}$	$7.5253 \cdot 10^{-2}$	$9.5431 \cdot 10^{-3}$
1	$3.4060 \cdot 10^{-1}$	$6.0246 \cdot 10^{-1}$	$2.1972 \cdot 10^{-1}$
2	$5.1797 \cdot 10^{-1}$	$2.6122 \cdot 10^{-1}$	$6.2665 \cdot 10^{-1}$
3	$6.5661 \cdot 10^{-2}$	$2.3048 \cdot 10^{-2}$	$8.3670 \cdot 10^{-2}$
4	$3.1286 \cdot 10^{-2}$	$2.1678 \cdot 10^{-2}$	$3.1648 \cdot 10^{-2}$
5	$1.2789 \cdot 10^{-2}$	$5.8293 \cdot 10^{-3}$	$1.5512 \cdot 10^{-2}$
6	$7.1636 \cdot 10^{-3}$	$7.3985 \cdot 10^{-3}$	$6.7379 \cdot 10^{-3}$
7	$2.3589 \cdot 10^{-3}$	$9.7566 \cdot 10^{-4}$	$2.6938 \cdot 10^{-3}$
8	$2.4155 \cdot 10^{-3}$	$1.1349 \cdot 10^{-3}$	$2.8687 \cdot 10^{-3}$
9	$7.0193 \cdot 10^{-4}$	$7.0350 \cdot 10^{-4}$	$5.6931 \cdot 10^{-4}$
10	$3.4110 \cdot 10^{-4}$	$3.0508 \cdot 10^{-4}$	$3.9023 \cdot 10^{-4}$

The problem was investigated by generating 1000 sample shapes using the parameters derived above. Model thermal lightcurves were generated by using the thermophysical model described by Lagerros (1997). This model takes into account heat conduction, the surface roughness, albedo spots, and irregular shapes. In order to study only the shape effects, most of these possibilities were neglected. In this simplified experiment, the surface temperature of each facet was taken to be in equilibrium with the insolation and zero if the facet was shadowed. The asteroids were placed at opposition in the main belt, and the Bond albedo was fixed at 10%. The spin vector was first fixed to be parallel with the axis of highest moment of inertia for the shapes, whereafter the bodies were oriented randomly with respect to the Sun.

The STM was fitted to the mean value of the thermal light curves, and STM diameters derived (assuming that the albedo of 10% somehow is known). The ratio between the STM radii and the mean radii (using the \tilde{r}_V -centre) of each shape was computed. The mean ratio of the radii is 0.95 with a 10% scatter. On the other hand, the average ratio of the volumes (or masses) of the fitted STM spheres to that of the irregular shape were 1.17, with a 33% scatter. The volume overestimate is the result of the fitting procedure, which in essence compares the projected

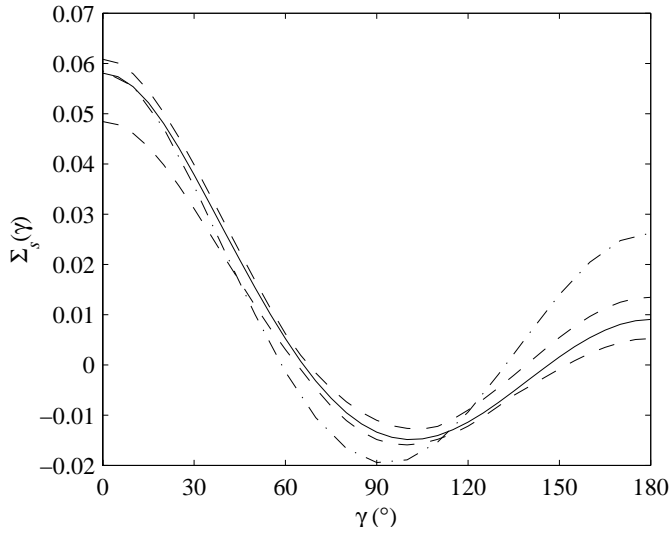


Fig. 5. The logradius covariance function $\Sigma_s(\gamma)$ inverted using all 14 shapes (solid line), with an error envelope (dashed lines; see text). Also shown is the covariance function computed with respect to the angular origins (dot-dashed line).

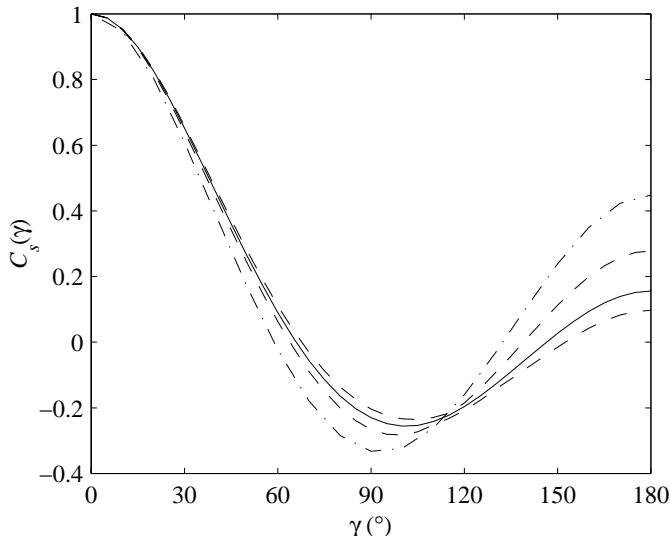


Fig. 6. The logradius correlation function $C_s(\gamma)$ for the 14 shapes (solid line), with an error envelope (dashed lines; see text). Also the correlation function computed with respect to the angular origins (dot-dashed line).

areas of the STM sphere and the irregular object. For a prescribed surface area, the sphere maximises the volume. This is not necessarily true for the *projected* area, but on the average it still produces an overestimate.

5. Conclusion

The shape models discussed here have many theoretical applications. For example, when deriving radiometric diameters, it is often common practise to assume spherical asteroids. In Sect. 4.3 a Monte Carlo approach is used in order to estimate the formal error introduced by using a sphere instead of the real

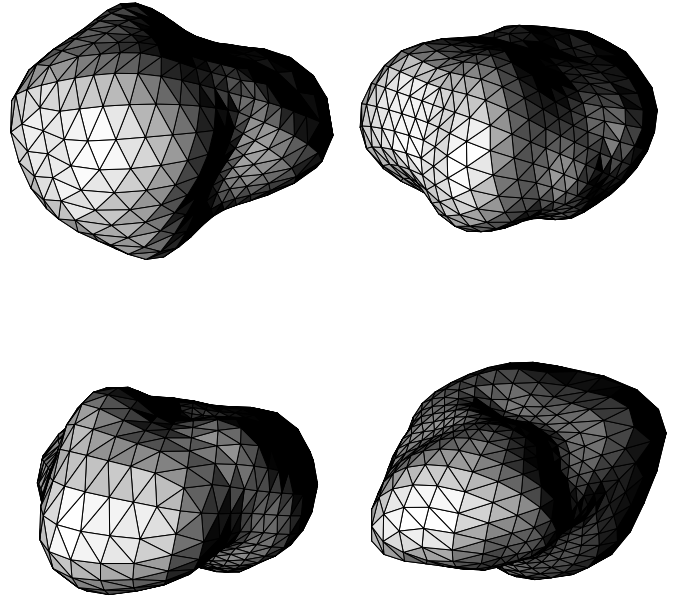


Fig. 7. Sample Gaussian spheres, using the derived covariance function in Fig. 5 and the first column in Table 4.

shape. There are a lot of other possibilities, for example, testing the shape inversion methods applied to visual light curves (Magnusson et al. 1989). Specific groups or families could be investigated by comparing the statistical properties of their lightcurves to synthetic lightcurves. It could be tested whether the shape or the reflection law is responsible for the observed increase in lightcurve amplitude at larger phase angles (Zappalà et al. 1990).

Already from the first analysis in Sect. 4.1 it is clear that the irregular objects of the solar system share some basic qualities in their shapes. The general behaviours in Figs. 1 and 2 are expected. A rough shape with high $\tilde{\sigma}$ requires large slopes $\tilde{\rho}$, and gravity does not allow large objects to be highly irregular. On the other hand, it is not immediately clear that almost all of the investigated shapes should have almost the same $\tilde{\rho}/\tilde{\sigma}$ -ratio. Together with the fitted curves in Fig. 2 the conclusion is that if the irregularities are scaled by the size, they are essentially the same (scale-invariant) over almost three orders of magnitude in size. The fact that there are outliers like 243 Ida and Proteus indicates that this is a real effect, rather than a self-fulfilling feature of the analysis itself.

Many of the foreseeable applications are described in Muinonen (1998) and Lagerros (1997). The present results enable a statistical study of the gravitational fields as well as the detailed study of spin-orbit coupling of small solar system bodies. Extensive simulations can be carried out in order to improve magnitude systems for asteroids, as well as different methods for asteroid spin vector determination. The present maximum likelihood estimates can be improved by accounting for the lightcurve data on asteroids. A fundamental question remains to be answered: why are the shapes of small solar system bodies similar in nature?

It is evident that the present number of sample shapes is still small, and it is our goal to improve the accuracy when new shape models are published. Furthermore, physical constraints on the shape irregularities can have a significant effect on the shape statistics. Future work will include more detailed hypothesis testing and sensitivity analysis, refining the present first results on the statistical shapes of small bodies.

References

- Aitchison, J. and Brown, J. A. C.: 1963, *The Lognormal Distribution*, University Press, Cambridge, U.K.
- Arfken, G.: 1970, *Mathematical Methods for Physicists*, Academic Press, New York, 2nd edition
- Babu, G.J. and Feidelson, E.D.: 1996, *Astrostatistics*, Chapman & Hall
- Hudson, R.S. and Ostro, S.J. 1994, *Science*, 263, 940
- Hudson, R.S. and Ostro, S.J. 1995, *Science*, 270, 84
- Lagerkvist, C.-I., Magnusson, P., Belskaya, I. et al.: 1996, *Asteroid Photometric Catalogue: Fourth Update*, Uppsala Astronomical Observatory
- Lagerros, J.S.V.: 1997, *A&A* 325(3), 1226
- Lamberg, L., Muinonen, K., Lumme, K., and Ylönen, J.: 1997, *Annals of Institute of Statistical Mathematics*, Submitted
- Lebofsky, L.A. and Spencer, J.R.: 1989, in R.P. Binzel, T. Gehrels, and M.S. Matthews (eds.), *Asteroids II*, pp. 128-147, Arizona University Press
- Magnusson, P., Barucci, M.A., Drummond, J.D. et al.: 1989, in R.P. Binzel, T. Gehrels, and M.S. Matthews (eds.), *Asteroids II*, pp. 66-97, The University of Arizona Press
- Muinonen, K.: 1996, *Earth, Moon, Planets* 72, 339
- Muinonen, K.: 1997, *Optical remote sensing of terrestrial surfaces: new sensors, advanced algorithms, and the opportunity for novel applications*, Submitted
- Muinonen, K., 1998, *A&A*, in press
- Muinonen, K., Nousiainen, T., Fast, P., Lumme, K., and Peltoniemi, J.I.: 1996, *J. Quant. Spectrosc. Radiat. Transfer* 55(5), 577
- Nousiainen, T.: 1997, Ph. Lic. thesis, University of Helsinki
- Nousiainen, T. and Muinonen, K.: 1997, *Journal of Atmospheric Science*, Submitted
- Peltoniemi, J.I., Lumme, K., Muinonen, K., and Irvine, W.M.: 1989, *Appl. Opt.* 28, 4088
- Stooke, P.J., 1992, *Earth, Moon, Planets* 56, 123
- Stooke, P.J.: 1993a, *Earth, Moon, Planets* 62, 199
- Stooke, P.J.: 1993b, *Earth, Moon, Planets* 63, 67
- Stooke, P.J.: 1994, *Earth, Moon, Planets* 65, 31
- Stooke, P.J.: 1997, http://europa.geog.uwo.ca/stooke_personalhomepage
- Stooke, P.J. and Lumsdon, M.P.: 1993, *Earth, Moon, Planets* 62, 223
- Thomas, P.C.: 1989, *Icarus* 77, 248
- Thomas, P.C., Belton, M.J.S., Carcich, B.: 1996, *Icarus* 120, 20
- Thomas, P.C., Binzel, R.P., Gaffey, M.J., Zellner, B.H. and Storrs, A.D.: 1997, *Icarus* 128, 88
- Thomas, P.C., Black, G.J., and Nicholson, P.D.: 1995, *Icarus* 117, 128
- Thomas, P.C., Veverka, J., Simonelli, D., Helfenstein, P. et al.: 1994, *Icarus* 107, 23
- Zappalà, V., Cellino, A., Barucci, A.M. et al.: 1990, *A&A* 231, 548